2017

Structural characterization of InAlAsSb/InGaAs/InP heterostructures for solar cells

N. Baladés
Universidad de Cádiz, nuria.balades@uca.es

M. Herrera
Universidad de Cádiz

D. L. Sales
Universidad de Cádiz

F. J. Delgado
Universidad de Cádiz

D. Hernández-Maldonado
SciTech Daresbury Campus

See next page for additional authors

Applied Surface Science 395 (2017) 98–104

Contents lists available at ScienceDirect

Applied Surface Science

journal homepage: www.elsevier.com/locate/apsusc

Structural characterization of InAlAsSb/InGaAs/InP heterostructures for solar cells

N. Baladés[a,*], M. Herrera[a], David L. Sales[a], F.J. Delgado[a], D. Hernández-Maldonado[b], Q.M. Ramasse[b], J. Pizarro[c], P. Galindo[c], M. González[d,e], J. Abell[d], S. Tomasulo[d], J.R. Walters[d], S.I. Molina[a]

[a] INNANOMAT Group, Departamento de Ciencia de los Materiales e I. M. y Q. I., Instituto Universitario de Investigación en Microscopía Electrónica y Materiales (IMEYMAT), CEI·MAR, Universidad de Cádiz, 11510 Puerto Real, Cádiz, Spain
[b] SuperSTEM Laboratory, SciTech Daresbury Campus, Keckwick Lane, Warrington WA4 4AD, UK
[c] Department of Computer Engineering, University of Cádiz, Avda. de la Universidad de Cádiz, no 10, 11519 Cádiz, Spain
[d] U.S Naval Research Laboratory, 4555 Overlook Ave. SW, Washington D.C. 20375, USA
[e] Sotera Defense Solutions, 430 National Business Pkwy # 100, Annapolis Junction, MD 20701, USA

ARTICLE INFO

Article history:
Received 22 January 2016
Received in revised form 13 July 2016
Accepted 13 July 2016
Available online 19 July 2016

Keywords:
InAlAsSb
High-efficiency
Solar cells
Multi-junction
HAADF-STEM

ABSTRACT

In this work, we have characterized by transmission electron microscopy techniques the structural properties of InAlAsSb/InGaAs/InP heterostructures, with target applications in high efficiency solar cells. Previous photoluminescence (PL)[1] analysis suggested the existence of compositional fluctuations in the active layer of these heterostructures. 220 bright field (BF)[2] diffraction contrast micrographs have revealed strong strain contrast in the InGaAs buffer layer, related to the existence of these compositional fluctuations. The effect of a decomposed buffer on the growth of the InAlAsSb layer has been analyzed through the simulation of the strain fields in the heterostructure using the finite elements method (FEM).[3] These simulations have shown that the strain in the buffer layer due to the compositional fluctuations only affects the first few nm of the InAlAsSb layer. The analysis by aberration corrected high angle annular dark field scanning transmission electron microscopy (HAADF-STEM)[4] and electron energy loss spectroscopy (EELS)[5] of the composition of the InAlAsSb layer reveals that any compositional fluctuation is only observed as an average effect, rather than in the form of clustering or atomically sharp transitions. The limitations of these techniques for the detection of small 3D compositional fluctuations are discussed.

1. Introduction

Solar energy is one of the most promising energy sources of this century, because of its carbon-free and inexhaustible nature. Over the past five decades, the research efforts in this field have been focused on raising the efficiency of solar cells. Developments such as the inverted metamorphic (IMM)[6] solar cell has allowed reaching efficiencies over 34% under 1 sun (AM0) illumination [1], although this design has shown to be limited by dislocations formed during the growth process [2]. Currently, the multi-junction (MJ)[7] technology based on lattice-matched III–V semiconductor alloys is considered as a very promising technology to enable ultra-high efficiency devices. In these MJ systems, each junction is optimized to match certain wavelength of the incident light through their tunable band gap energies, so high energy conversion efficiencies are expected [3]. In this context, the quaternary InAlAsSb is a promising alloy for the top junction of the InP-based triple-junction concentrator cell design. This material can achieve direct band gaps ranging from 1.45 to ~1.8 eV, which is expected to provide ultra-high efficiency in conversion of light under concentrated (AM 1.5D) illumination [4].

The InAlAsSb alloy is a relatively immature material, and its structural and optoelectronic properties need to be analyzed in

* Corresponding author.
E-mail address: nuria.balades@uca.es (N. Baladés).
[1] PL: photoluminescence.
[2] BF: bright field.
[3] FEM: the finite elements method.
[4] HAADF-STEM: high angle annular dark field scanning transmission electron microscopy.
[5] EELS: electron energy loss spectroscopy.
[6] IMM: inverted metamorphic.
[7] MJ: multi-junction.

http://dx.doi.org/10.1016/j.apsusc.2016.07.094
0169-4332/

detail. This material is expected to have a bandgap value of about 1.8 eV. However, preliminary studies by the authors have shown a discrepancy between the bandgap values extracted by PL measurement and by ellipsometry [5]. On the other hand, initial PL studies of this quaternary layer have revealed a red-shift in the peak emission energy as a function of the incident power density, along with a significant deviation from its expected bandgap [6]. These results suggest spatially-indirect recombination related to compositional fluctuations. In that analysis, the studied InAlAsSb layers were grown on InP using InGaAs buffer layers. The advantage of using InGaAs buffer layers with regard to other commonly used materials such as InAlAs is that InGaAs has lower bandgap and higher mobility than InAlAs, leading to a reduced series resistance value on the final device. In the PL study, the main reason for using InGaAs buffers is to block the PL emission from the substrate (1.35 eV at room temperature), to avoid overlapping with the PL emission from the InAlAsSb layer. However, the InGaAs alloy has a known tendency to spinodal decomposition under certain growth conditions [7–9]. The structural characteristics of the buffer layer could have an effect on the growth of the InAlAsSb layer, and potentially on its PL emission properties, therefore it should be considered in the understanding of the behavior of this alloy.

In this work, we have studied the structural properties of InAlAsSb/InGaAs/InP heterostructures in order to shed some light on the PL characteristics observed previously. In particular, the compositional distribution in the InAlAsSb layer has been analyzed with atomic column resolution using HAADF-STEM EELS in an effort to ascertain the presence of localized compositional changes (clusters, etc...), which would drastically affect the absorption properties of the layer. Furthermore, the effect of using InGaAs buffer layers with phase separation on the strain of the InAlAsSb layer has been analyzed using the finite element method.

2. Material and methods

The studied samples consist of a 1 μm thick layer of $In_{0.31}Al_{0.69}As_{0.82}Sb_{0.18}$ grown on an $In_{0.53}Ga_{0.47}As$ buffer layer with thickness of 200 nm on an InP substrate. The $In_{0.31}Al_{0.69}As_{0.82}Sb_{0.18}/In_{0.53}Ga_{0.47}As/InP$ heterostructure is lattice-matched to InP. The lattice constants values are 5.86 Å, 5.87 Å and 5.87 Å respectively. The heterostructure has been grown by molecular beam epitaxy (MBE),[8] in an As-Sb Veeco Gen II system. A specimen has been thinned down to electron transparency for transmission electron microscopy (TEM)[9] cross-sectional analyses by mechanical grinding and Ar^+ ion milling using a precision ion polishing system (PIPS)[10] with a beam tilt of 4° and beam energy of 3.5 kV. Finally, the specimen has been plasma cleaned before the TEM analysis to reduce the effect of the electron beam deposition of parasitic carbohydrates on the specimen surface [10].

The TEM diffraction contrast study has been performed using a JEOL 1200EX transmission electron microscope operating at 120 kV. The HAADF images and the EELS spectrum images have been acquired simultaneously using an aberration corrected Nion UltraSTEM, operating at 100 kV with a convergence semi-angle of 32 mrad. The microscope is equipped with a Gatan Enfina EELS spectrometer and a HAADF detector with inner and effective outer semi-angles of 80 mrad and 185 mrad. EEL spectra were collected using an aperture semi-angle of 36 mrad. The resolution limit of the microscope is about 0.8 Å.

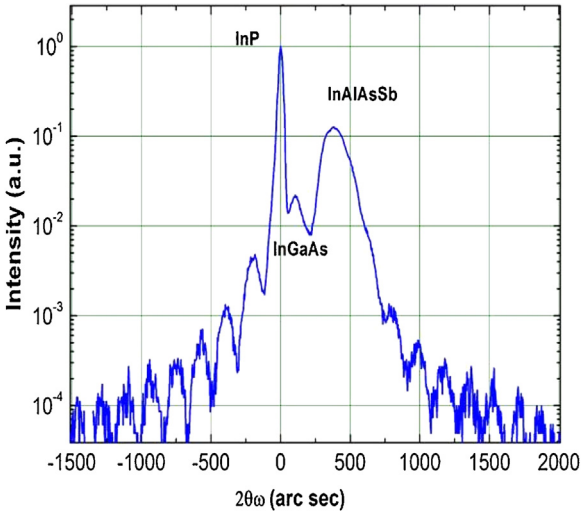

Fig. 1. XRD data corresponding to the InAlAsSb/InGaAs/InP heterostructure.

FEM modelling has been carried out in order to simulate the strain in a three-dimensional heterostructure. The model has been defined using combinations of three volumes or domains. The first domains consist of $50 \times 50 \times 50\,nm^3$ corresponding to the substrate and it is assumed to be pure InP. The second one consists of $50 \times 50 \times 200\,nm^3$ of $In_xGa_{1-x}As$. In the domain corresponding to the InGaAs layer, composition fluctuations have been included introducing a set of sinusoidal functions with different phases along the growth direction, where In and Ga compositions vary ±5% from their average values (53% and 47% respectively). Vegard's law has been applied to estimate the elastic constants values at different compositions. The third domain consists of $50 \times 50 \times 200\,nm^3$ of $In_{0.31}Al_{0.69}As_{0.82}Sb_{0.18}$. Elastic constants have been taken from the literature [11]. The periodicity of the structure has been chosen to be 50 nm and it has been taken into account by applying the appropriate boundary conditions. To introduce the misfit at the interface between the layers and the substrate, the initial strain has been assumed to be $\varepsilon_0 = \frac{a-aInP}{aInP}$, being therefore dependent on the composition. The basic mesh distribution for finite element calculation is usually calculated using the Delaunay algorithm, as it can be applied to all geometry objects. The strain field has then been obtained from the model by solving the equations of the anisotropic elastic theory by FEM.

The column to column compositional analysis of the HAADF images has been carried out by applying the quantitative HAADF image analysis algorithm (*qHAADF*)[11] available to run using the *Digital Micrograph* (GATAN™) software, available from *HREM Research Inc.* The *qHAADF* algorithm to analyse the normalized integrated intensities in HAADF images was developed by Sergio I. Molina et al. [12] Here, after an automatic finding of the intensity peaks using 2D filtering (Bragg, Wiener...) and cubic interpolation techniques [13], the integrated intensities in selected areas of the HAADF images are measured and mapped.

3. Results and discussion

The sample has been initially studied by X-ray diffraction (XRD) in order to verify the crystalline structure. Fig. 1 shows the XRD obtained from the InAlAsSb/InGaAs/InP heterostructure. For this sample, the InAlAsSb epilayer peak appears within 380″ of the substrate peak. Assuming that the layers are coherently strained, this

[8] MBE: molecular beam epitaxy.
[9] TEM: transmission electron microscopy.
[10] PIPS: precision ion polishing system.
[11] qHAADF quantitative HAADF image analysis algorithm.

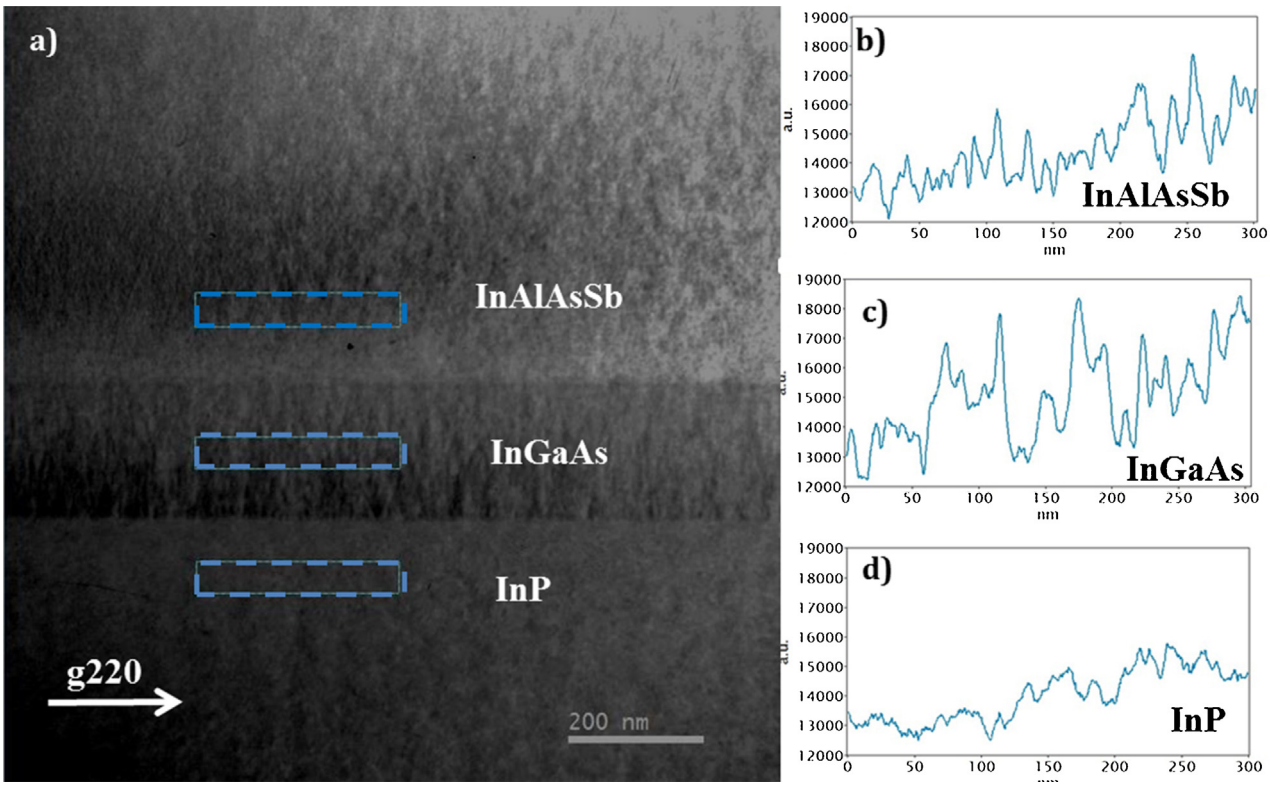

Fig. 2. a) 220BF TEM micrograph of the InAlAsSb/InGaAs/InP sample, revealing the presence of strain contrast in the InGaAs and InAlAsSb layers. Intensity profiles taken from the InAlAsSb b), the InGaAs c) and the InP d) layers, along the regions marked with blue rectangles in Fig. 2a). (For interpretation of the references to color in this figure legend, the reader is referred to the web version of this article.)

value corresponds to an out of plane lattice constant mismatch with respect to the substrate of 1490 parts per million (ppm) or alternatively, less than 0.15% lattice mismatch, which allows a considerably amount of epitaxial material to be grown without any defects.

Fig. 2a shows a 220 bright field (BF) TEM micrograph of the InAlAsSb sample with the InGaAs buffer layer, where no dislocations or any other structural defect can be found. As it can be observed, the InGaAs layer exhibits some contrast oscillations, more intense in the [110] direction than in the growth direction [001]. Some contrasts can also be found in the InAlAsSb layer, although these are not so evident. Intensity profiles have been taken and averaged from the blue rectangles included in Fig. 2a in the InAlAsSb active layer (Fig. 2b), in the InGaAs buffer layer (Fig. 2c) and in the InP substrate (Fig. 2d). These profiles show that the lateral contrast variations found in the ternary layer are stronger than those found in the InAlAsSb layer and in the InP substrate. These contrast oscillations are associated with lateral strain variations, which are postulated to relate to composition fluctuations. The presence of composition fluctuations in InGaAs and other ternary semiconductor compounds obtained by epitaxial growth have been widely reported in the literature [8,9,14,15] and they have been attributed to a process of spinodal decomposition [16]. These compositional fluctuations depend on the growth temperature, the alloy composition and the growth rate [17,18] and some authors believe that they are thermally activated [19,20]. With regard to the quaternary InAlAsSb layer, it should be mentioned that strain contrast as strong as that found in the InGaAs layer has not been observed. This indicates that possible compositional fluctuations in the quaternary layer, as those suggested by the PL measurements [6], would not cause such large variation in the lattice parameter through the structure than in InGaAs.

The existence of composition fluctuations in the InGaAs buffer layer derived from the diffraction contrast analysis above could affect the growth of the active quaternary layer. In order to shed some light on the effect of some heterogeneities in the buffer layer on the InAlAsSb layer, we have simulated the strain of the heterostructure by FEM modelling. For this, we have built a model formed by three different domains: the InP substrate, the InGaAs buffer layer and the InAlAsSb active layer, as described in the Methods section. In the domain corresponding to the InGaAs layer, composition fluctuations have been included introducing a set of sinusoidal functions with different phases along the growth direction, where In composition varies between $53 \pm 5\%$ and Ga between $47 \pm 5\%$. The amplitude of these compositional fluctuations in the InGaAs layer is an important parameter to be set in this model. However, despite the fact that this material has been widely studied in the literature, experimental estimates of this amplitude parameter have not been published. Studies of InGaAs/InP systems have shown that the amplitude of the fine modulation wavelength decreases with growth temperature, In concentration or thickness increase [14]. McDevitt et al. found an increase in the fine modulation wavelength with growth temperature in InGaAsP grown on InP, regardless of their composition [21]. Bartel et al. found a parabolic increase of the fluctuation amplitude in InGaN systems when the In concentration is increased [17]. Nevertheless, these studies do not include a quantification of the magnitude of small compositional fluctuations. This is due to the complexity of the compositional distribution, given that it is expected to consist in 3D small variations. In this sense, Ga enrichment areas about 4–6% over the nominal composition have been reported in InGaAs graded buffers grown on offcut wafers, measured using Moiré fringe spacing [22]. In order to investigate the effect of strong composition fluctuations in the InGaAs buffer layer on the growth of the InAlAsSb layer, we have considered In fluctuations relatively high, of ±5%,

and of the same order of magnitude of that obtained in Ref. [22]. These composition variations induce a strain of 5% on the top surface of the buffer layer before including the quaternary layer. This is a considerable value, because strain variations of about 3% are able to induce the formation of structural defects in InGaAs/AlGaAs quantum dot (QDs) [23], although dislocations have not been found in our study. However, we have found a strong reduction in the strain values of the InAlAsSb layer with the distance to the InGaAs surface, as shown below.

Fig. 3 shows the strain maps calculated with regard to the InP substrate in the growth direction in planes parallel to the growth plane [001], for different positions in the InAlAsSb/InGaAs heterostructure: at the InAlAsSb/InGaAs interface (a) and at 5 nm (b), 10 nm (c) and 15 nm (d) from the buffer layer. As it can be observed, the strain in the quaternary layer at the interface is around ±1%. However, and as it can be observed, when moving upwards in the structure the strain in the quaternary layer is rapidly reduced to values of around ±0.4%, 0.15% and 0.05% for the distances showed in Fig. 3, respectively, being practically negligible at 50 nm (about 9.5×10^{-4}%). In light of the results obtained, it can be concluded that the strain due to the composition fluctuations in the InGaAs layer affects only the initial monolayers of the InGaAs layer. The chemical potential of the growth surface at the beginning of the InAlAsSb growth could be affected by small distortions, leading to light compositional fluctuations. Nevertheless, this influence is not significant with respect to the total volume of the quaternary layer (which is 1 μm thick) given that the PL emission analyzed previously is expected to originate from the overall InAlAsSb layer. Therefore, our results suggest that, in terms of strain propagation, the composition fluctuations predicted by the PL measurements [24] are not expected to be caused by the spinodally decomposed InGaAs buffer layer.

In order to obtain further information on the composition distribution of the InAlAsSb layer both at the interface with the InGaAs layer and in regions far from the interface, an analysis by aberration corrected HAADF has been carried out. In HAADF, the intensity obtained is, to a good approximation, proportional to the sum of the square of the atomic numbers (Z) of the atoms in a given column, providing useful compositional information. Fig. 4a shows a HAADF image taken along the [110] zone axis of the InAlAsSb/InGaAs interface. As it can be observed, clear intensity variations that could be correlated to compositional fluctuations are not found either in the InGaAs layer or the InAlAsSb layer. In order to analyse in more detail the intensity in the image, the *qHAADF* algorithm has been applied [12]. In this work, this algorithm is used to calculate the integrated intensity around the cations (I_c) and the anions (I_a) columns in the material, and Fig. 4b and c shows the obtained intensity maps, respectively. As it can be observed, small fluctuations in the intensity values are found both in the InAlAsSb and the InGaAs layers. In order to compare the dispersion of the obtained results, we have calculated the correlation coefficient C_v (defined as the ratio between the standard deviation and the mean intensity value) in the ternary layer, the quaternary layer and the substrate and we have obtained a value of $C_v \approx 2\%$ in all layers. Thus, the fluctuations observed in the regions of interest are of the same order of magnitude than those found in the InP substrate, which has uniform composition, therefore they can be related to small variations in the sample thickness and fall into the error of the measurement. Because of this, no significant composition fluctuations can be derived from the developed HAADF analysis. Different specimens with variable thickness have been analyzed, studying both regions close to the interface and regions far away from it, obtaining the same result. It is worth mentioning that, as it can be observed, the intensity in the ternary layer is higher than in the quaternary layer everywhere, what is related to a higher average Z number in InGaAs than in InAlAsSb. This is something widely observed in HAADF images, and it is related to the *cross-talk* between the atomic columns. In our study, we focus on finding variations in intensity within each of the layers that could evidence composition fluctuations. In these variations, the difference found between the average intensity of the ternary and the quaternary layers are not expected to have any effect.

The composition in the heterostructure has also been analyzed by EELS. Elemental distribution maps corresponding to the area of the InGaAs/InP interface marked with a green rectangle in the HAADF image of Fig. 5a) have been obtained by the analysis of the core loss spectrum signals. Fig. 5b) shows the normalized elemental map corresponding to the In $M_{4,5}$ ionisation edge (onset at 443.1 eV). This map has been obtained by integrating the edge intensity over a 89 eV window after subtraction of the decaying background using a power-law fit over a region immediately in front of the core loss edge, and then normalizing it with the average In signal in the substrate. Fig. 5c) shows a map of t/λ, (where t is the thickness of the sample and λ the inelastic mean free path), showing that the analyzed area correspond to a thin region of the sample with a small thickness gradient. As it can be observed in Fig. 5b), small variations in the In $M_{4,5}$ signal can be observed with Cv ≈6.8%. However, small fluctuations of the same magnitude are also found in the InP substrate, with Cv ≈5%. The In composition in the InP substrate is known to be homogeneous and therefore the small fluctuations observed in the active layer are not thought to be related to real composition changes but to the inherent error of the measurement. The variations found both in the InGaAs and the InP layers are of the same order of magnitude, and this indicates that they do not show significant compositional changes in the InGaAs layer, which is the same result derived from the HAADF-STEM analysis. Fig. 5d shows a HAADF image of the InAlAsSb layer, and Fig. 5e shows the normalized In $M_{4,5}$ signal maps corresponding to the area included in the green square marked in the image. Fig. 5f shows a map of t/λ, showing that the analyzed area correspond to a thin region of the sample. Although small fluctuations have again been observed in the In signal obtained from the InAlAsSb layer in Fig. 5e (Cv ≈6.4%), these variations also fall within the error of the measurement, therefore compositional changes are not evidenced from the EELS analysis employed here.

In the analysis carried out by HAADF and EELS, data pointing to the existence of compositional fluctuations in the InAlAsSb and the InGaAs layers studied have not been clearly obtained. However, the analysis by diffraction contrast of the structure has shown clear strain contrast in the InGaAs layer, likely related to the existence of compositional variations. Also, previous studies by PL point to the existence of compositional fluctuations in the InAlAsSb layer [6]. The reasons for the results obtained could lie in the projected 2D nature of the analyses developed by most TEM techniques, given that in these analyses the 3D features of a specimen are projected on a 2D plane. Because of this, the composition of each atomic column is averaged through the specimen thickness. If the regions of different composition have a small size in comparison to the specimen foil, when the electron beam is channelled through a particular atomic column of the material, it can go through several of these domains. Even when the data collection is different in HAADF and EELS, this effect can produce that in both techniques the results only show an averaged value corresponding to part or the whole atomic columns in the specimen thickness. This average value could be similar for different regions of the specimen, and thus the results would not exhibit possible 3D small compositional fluctuations present in the material. The magnitude of the compositional variations in the structure is also an important parameter to be taken into account. For example, the difference between the number of In atoms in an $In_xGa_{1-x}As$ specimen foil 30 nm thick in a [110] projected cation column when its composition x varies from 0.53 to 0.59 is only of three atoms. Therefore, the detection lim-

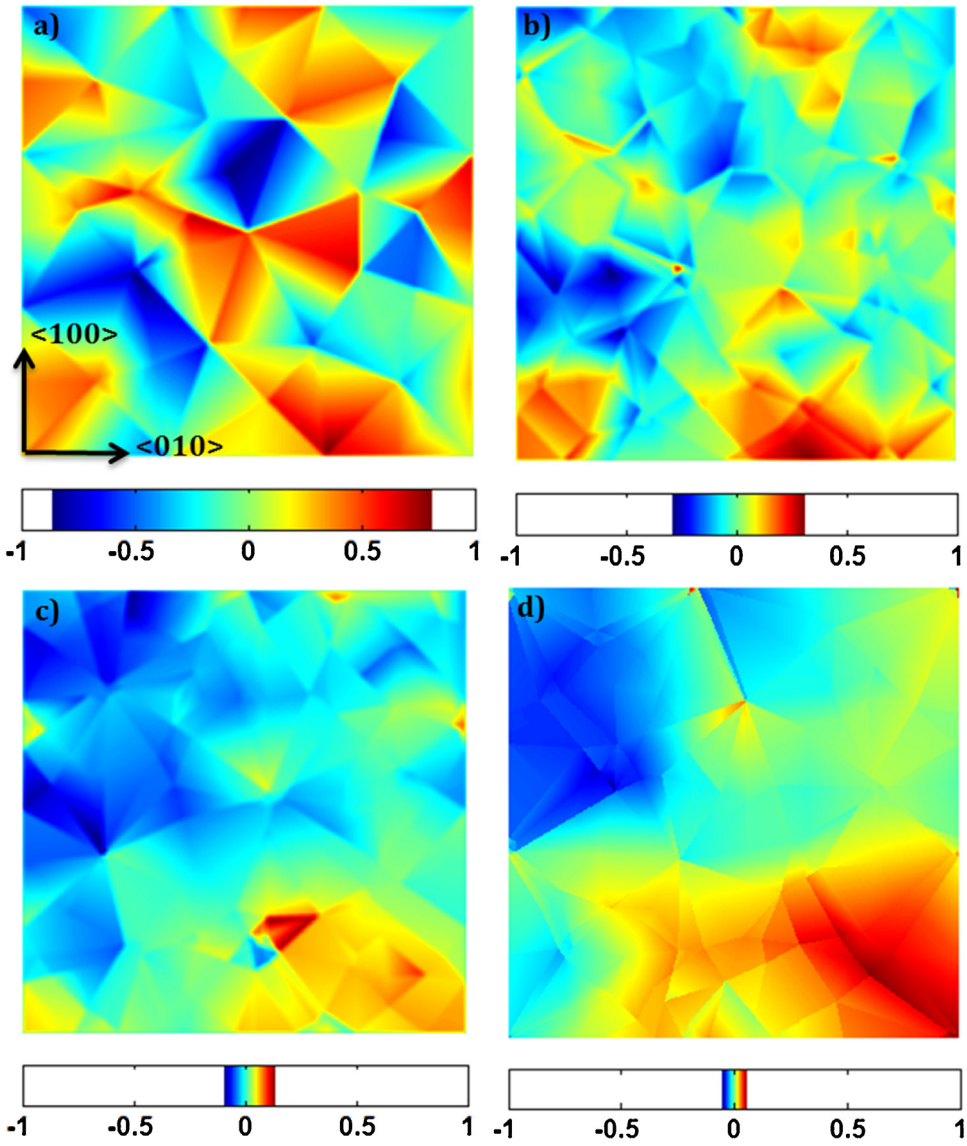

Fig. 3. Evolution of the strain fields along the growth direction in the heterostructure: at the InAlAsSb/InGaAs interface a), and at 5 nm b), 10 nm c) and 15 nm d) from the interface; a notable reduction of the strain with the distance to the interface is evidenced. Left, schematic model structure with the position of these planes.

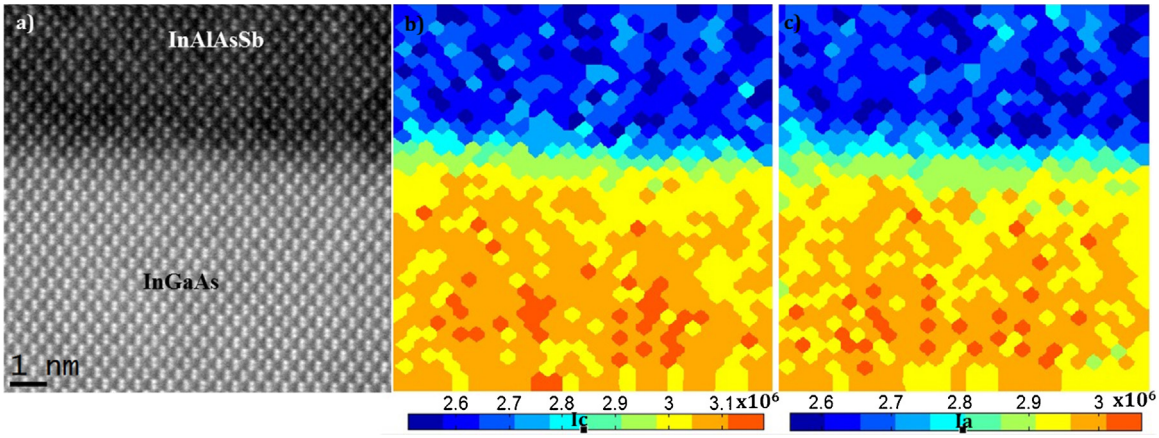

Fig. 4. a) HAADF image of the InAlAsSb/InGaAs interface; b) Colour map of the integrated cation columns intensity and c) integrated anion columns intensity, both obtained from the HAADF image in a).

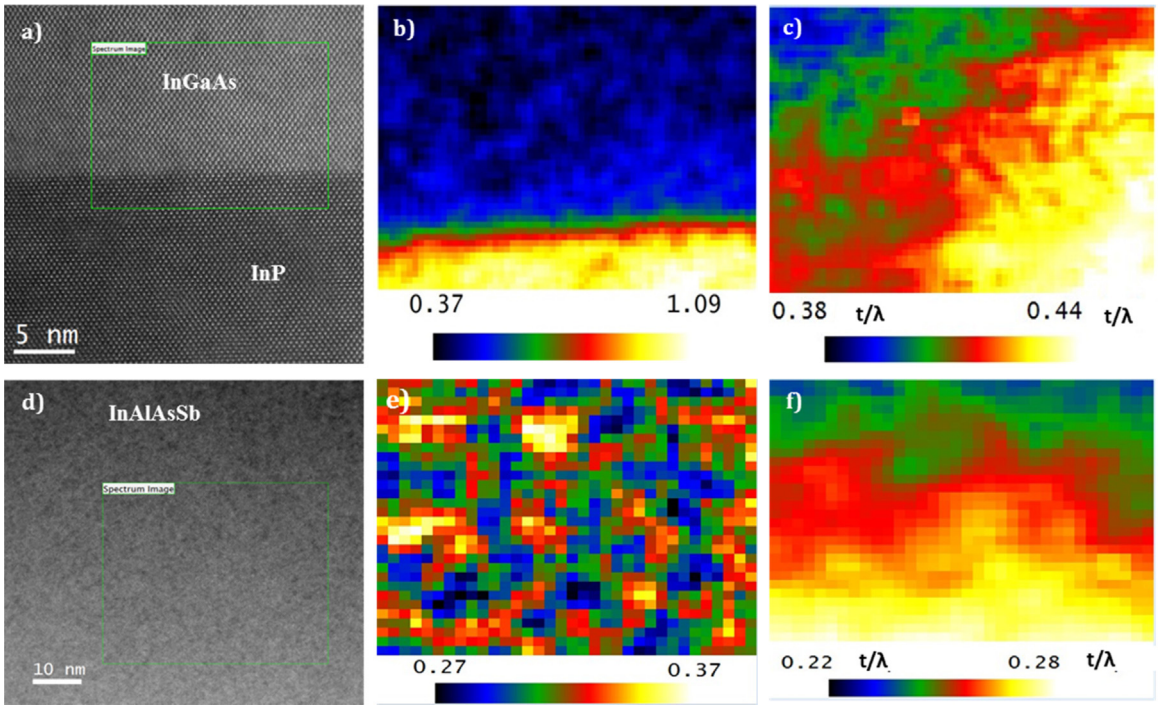

Fig. 5. a) HAADF image of the InGaAs/InP interface; b) normalized In $M_{4,5}$ signal map corresponding to the region marked with a green rectangle in a); c) t/λ map corresponding to the region marked with a green rectangle in a); d) HAADF image of the InAlAsSb active layer; e) normalized In $M_{4,5}$ signal map corresponding to the region marked with a green rectangle in d); e) t/λ map corresponding to the region marked with a green rectangle in d). (For interpretation of the references to color in this figure legend, the reader is referred to the web version of this article.)

its of the techniques used in the composition measurements play an important role. In order to obtain an estimation of the detection limit in our HAADF experiments, we have extracted some approximate compositional information from the HAADF intensity values obtained in our study considering the method proposed by Mukherjee et al. [15] For the InP substrate, we have obtained a variability of ±2% in the measured In composition, that can be considered as the error of the method. This means that independent clusters with In enrichments smaller than 2% could not be measured with this experimental conditions. In EELS, considering that in the InP layer the In average counts recorded represent a composition of 100% In, we have obtained a variability of 6%In, indicating that clusters with composition smaller than this could not be detected. Ideally, to establish detection limits in HAADF or EELS, the measurements should be done with alloys chemically homogeneous such as binary compounds. However, even the atomic order of the atoms in an atomic column with the same composition could affect the value of HAADF intensity images limiting the accuracy of the measurement [25]. Using an automated process of HAADF image processing, it has been found that the measurement of individual column ratios in AlAs/GaAs has an overall standard error of 5–6% [26]. In some studies, the use of image simulations has allowed determining elements composition with a high accuracy. Thus, the comparison of experimental and simulated HAADF images has allowed the measurement of N compositions in GaNAs quantum wells with an accuracy of 1% [27], and the observation of variations of two atoms in pure Au films [28]. The quantification of the compositional distribution by HAADF when the material is an alloy with more than one type of element in each sublattice such as InAlAsSb has additional difficulties. Although the electron beam is expected to channel through the atomic columns, often it can be displaced briefly to the neighbouring atomic columns (known as the *cross-talk*). In the resulting HAADF image, the information from different atomic columns (each with non-uniform compositional distributions) can be mixed. This has been faced in the literature by using a combination of TEM techniques to measure the composition [29–31]. With regard to EELS, usual compositional measurement accuracies are around 10% [32]. However, by using careful methodologies including the determination of the noise performance of the detection system and the influence of different instrumental configurations on the quantification results, the detection of Cr concentrations in Al_2O_3 down to 0.03% for a given optimal determined set of analysis parameters has been reported [33]. Although this technique seems more promising for the analysis of quaternary alloys, the detection of small 3D compositional fluctuations would require an optimization of the specimen thickness taking into account the size of the rich and poor volumes in the material. However, for the appropriate analysis of the material, retaining some bulk-like shape is needed, otherwise the sample does not reflect accurately the as-grown properties of the material, due for instance to thin film relaxation, surface chemical changes (oxidation) or defects created during sample preparation (dislocation, heavy ion implantation etc.). While ultra-thin samples are possible for test cases (such as those mentioned above), in the case of real layers the usable thickness range is somehow limited. The use of techniques of analysis that provide 3D elemental information on a material at atomic scale would be of great importance for the analysis of a complex system such as the InAlAsSb quaternary alloy. The analysis by Atom Probe Tomography of this material is in progress in order to quantify the compositional distribution in the heterostructure. This will allow, on the one hand, setting detection limits for the HAADF and EELS experiments developed, and on the other hand, understanding the PL behavior of this novel alloy, allowing the progress of MJ solar cells.

4. Conclusion

The analysis by diffraction contrast TEM of an InAlAsSb/InGaAs/InP heterostructure has shown the presence of strain contrast likely related to composition fluctuations in the

InGaAs buffer layer, and not in the InAlAsSb active layer. Simulations using FEM modelling of the strain in the quaternary layer due to compositional fluctuations in the buffer layer have shown that it only affects some few nm of the InAlAsSb layer grown close to the interface with the buffer layer. This indicates that the effect of the InGaAs buffer on the compositional distribution of the 1 μm thick InAlAsSb layer is expected to be small, and likely not responsible for the PL behavior observed previously in this alloy. The analysis by aberration corrected HAADF and EELS of this sample has not shown significant composition fluctuations in the InAlAsSb and InGaAs layers, confirming that if present, any chemical effect if extremely small. The projection of the 3D features of a sample on a 2D plane that occurs in TEM analyses could be an important limitation for the analysis of 3D small compositional fluctuations in semiconductor heterostructures.

Acknowledgements

This work was supported by ONRG through the NICOP research grant N62909-14-1-N244, Spanish MINECO (projects TEC2014-53727-C2-2-R and CONSOLIDER INGENIO 2010 CSD2009-00013), and Junta de Andalucía (PAI research group TEP-946). Co-funding from FEDER-EU is also acknowledged. The SuperSTEM Laboratory is the U.K. National Facility for Aberration-Corrected STEM, supported by the Engineering and Physical Sciences Research Council (EPSRC).

References

[1] P. Patel, D. Aiken, A. Boca, B. Cho, D. Chumney, M.B. Clevenger, A. Cornfeld, N. Fatemi, Y. Lin, J. McCarty, F. Newman, P. Sharps, J. Spann, M. Stan, J. Steinfeldt, C. Strautin, T. Varghese, Experimental results from performance improvement and radiation hardening of inverted metamorphic multijunction solar cells, IEEE J. Photovolt. 2 (2012) 377–381.
[2] T. Takamoto, T. Agui, A. Yoshida, K. Nakaido, H. Juso, K. Sasaki, K. Nakamora, H. Yamaguchi, T. Kodama, H. Washio, M. Imaizumi, M. Takahashi, World's highest efficiency triple-junction solar cells fabricated by inverted layers transfer process, 35th Ieee Photovoltaic Specialists Conference (2010) 412–417.
[3] M.A. Green, Solar cell efficiency tables (version 46) (vol 23 pg 805, 2015), Prog. Photovolt. 23 (2015) 1202.
[4] M. Gonzalez, M.P. Lumb, M.K. Yakes, C.G. Bailey, J.G. Tischler, R. Hoheisel, J. Abell, I. Vurgaftman, J. Meyer, S. Maximenko, P.P. Jenkins, S.I. Molina, F.J. Delgado-Gonzalez, D. Bahena, A. Ponce, J.G.J. Adams, M. Fuhrer, N. Ekins-Daukes, R.J. Walters, Towards high efficiency multi-Junction solar cells grown on InP substrates, 2013 Ieee 39th Photovoltaic Specialists Conference (Pvsc) (2013) 145–148.
[5] M. Gonzalez, M.P. Lumb, L.C. Hirst, S. Tomasulo, J.G. Tischler, W. Yoon, J. Abell, I. Vurgaftman, M.F. Bennett, K.J. Schmieder, N.A. Kotulak, M.K. Yakes, J.R. Meyer, R.J. Walters, Rapid thermal annealing of InAlAsSb lattice-matched to InP for top cell applications, 2015 Ieee 42nd Photovoltaic Specialist Conference (2015).
[6] L.C. Hirst, M.P. Lumb, J. Abell, C.T. Ellis, J.G. Tischler, I. Vurgaftman, J.R. Meyer, R.J. Walters, M. Gonzalez, Spatially indirect radiative recombination in InAlAsSb grown lattice-matched to InP by molecular beam epitaxy, J. Appl. Phys. 117 (2015).
[7] J.W. Cahn, On spinodal decomposition, Acta Metall. Mater. 9 (1961) 795–801.
[8] T.L. McDevitt, F.S. Turco, M.C. Tamargo, S. Mahajan, D.E. Laughlin, V.G. Keramidas, W.A. Bonner, Effects of substrate orientation on phase-separation in ingaas and ingaasp epitaxial layers, Inst. Phys. Conf. Ser. (1989) 173–180.
[9] F. Peiro, A. Cornet, J.R. Morante, M. Beck, M.A. Py, Surface roughness in InGaAs channels of high electron mobility transistors depending on the growth temperature: strain induced or due to alloy decomposition, J. Appl. Phys. 83 (1998) 7537–7541.
[10] R.F. Egerton, P. Li, M. Malac, Radiation damage in the TEM and SEM, Micron 35 (2004) 399–409.
[11] N. Bouarissa, Elastic properties of AlxGa1-xAsySb1-y lattice matched to different substrates, Mater. Chem. Phys. 78 (2002) 271–277.
[12] S.I. Molina, D.L. Sales, P.L. Galindo, D. Fuster, Y. Gonzalez, B. Alen, L. Gonzalez, M. Varela, S.J. Pennycook, Column-by-column compositional mapping by Z-contrast imaging (vol 109 pg 172, 2009), Ultramicroscopy 109 (2009) 1315.
[13] P.L. Galindo, J. Pizarro, E. Guerrero, M.P. Guerrero-Lebrero, G. Scavello, A. Yanez, B.M. Nunez-Moraleda, J.M. Maestre, D.L. Sales, M. Herrera, S.I. Molina, A methodology for the extraction of quantitative information from electron microscopy images at the atomic level, in: P.D. Nellist (Ed.), Electron Microscopy and Analysis Group Conference 2013 (2014).
[14] M. Herrera, D. Gonzalez, M.U. Gonzalez, Y. Gonzalez, L. Gonzalez, R. Garcia, Composition modulation in low temperature growth of InGaAs/GaAs system: influence on plastic relaxation, Microchim. Acta 145 (2004) 63–66.
[15] K. Mukherjee, A.G. Norman, A.J. Akey, T. Buonassisi, E.A. Fitzgerald, Spontaneous lateral phase separation of AlInP during thin film growth and its effect on luminescence, J. Appl. Phys. 118 (2015).
[16] A. Lahiri, Effect of Epitaxial Strain on Phase Separation in Thin Films, Arxiv_1310.5899v1, (2013).
[17] T.P. Bartel, P. Specht, J.C. Ho, C. Kisielowski, Phase separation in inxGa1-xN, Philos. Mag. 87 (2007) 1983–1998.
[18] Z.-c. Ye, Y.-c. Shu, X. Cao, L. Gong, B. Pi, J.-h. Yao, X.-d. Xing, J.-j. Xu, Thermodynamic analysis of growth of ternary III-V semiconductor materials by molecular-beam epitaxy, Trans. Nonferrous Metals Soc. China 21 (2011) 146–151.
[19] P. Roura, A. Vila, J. Bosch, M. Lopez, A. Cornet, J.R. Morante, D.I. Westwood, Atomic diffusion induced by stress relaxation in InGaAs/GaAs epitaxial layers, J. Appl. Phys. 82 (1997) 1147–1152.
[20] K. Muraki, S. Fukatsu, Y. Shiraki, R. Ito, Sufarce segregation of In atoms during molecula-beam epitaxy and its influence on the energy-levels in InGaAs/GaAs quantum-wells, Appl. Phys. Lett. 61 (1992) 557–559.
[21] T.L. Mcdevitt, S. Mahajan, D.E. Laughlin, W.A. Bonner, V.G. Keramidas, Surface Phase Separation and Ordering in Compound Semiconductor Alloys, MRS Proc. 198 (1990) 609, http://dx.doi.org/10.1557/PROC-198-609.
[22] N.J. Quitoriano, E.A. Fitzgerald, Relaxed, high-quality InP on GaAs by using InGaAs and InGaP graded buffers to avoid phase separation, J. Appl. Phys. 102 (2007).
[23] D.L. Sales, J. Pizarro, P.L. Galindo, R. Garcia, G. Trevisi, P. Frigeri, L. Nasi, S. Franchi, S.I. Molina, Critical strain region evaluation of self-assembled semiconductor quantum dots, Nanotechnology 18 (2007).
[24] T. Nuytten, M. Hayne, B. Bansal, H.Y. Liu, M. Hopkinson, V.V. Moshchalkov, Charge separation and temperature-induced carrier migration in Ga1-xInxNyAs1-y multiple quantum wells, Phys. Rev. B 84 (2011).
[25] E. Carlino, Quantitative Z-contrast atomic resolution studies of semiconductor nanostructured materials, in: P.D. Walther, J.L. Nellist (Eds.), 16th International Conference on Microscopy of Semiconducting Materials (2010).
[26] P.D. Robb, A.J. Craven, Column ratio mapping: a processing technique for atomic resolution high-angle annular dark-field (HAADF) images, Ultramicroscopy 109 (2008) 61–69.
[27] T. Grieb, K. Mueller, O. Rubel, R. Fritz, C. Gloistein, N. Neugebohrn, M. Schowalter, K. Volz, A. Rosenauer, Iop, determination of nitrogen concentration in dilute GaNAs by STEM HAADF Z-contrast imaging, in: T. Walther, P.A. Midgley (Eds.), 17th International Conference on Microscopy of Semiconducting Materials 2011 (2011).
[28] J.M. LeBeau, S.D. Findlay, L.J. Allen, S. Stemmer, Standardless atom counting in scanning transmission electron microscopy, Nano Lett. 10 (2010) 4405–4408.
[29] T. Grieb, K. Mueller, E. Cadel, A. Beyer, M. Schowalter, E. Talbot, K. Volz, A. Rosenauer, Simultaneous quantification of indium and nitrogen concentration in InGaNAs using HAADF-STEM, Microsc. Microanal. 20 (2014) 1740–1752.
[30] J.M. Tilli, H. Jussila, K.M. Yu, T. Huhtio, M. Sopanen, Composition determination of quaternary GaAsPN layers from single X-ray diffraction measurement of quasi-forbidden (002) reflection, J. Appl. Phys. 115 (2014).
[31] F.F. Krause, J.-P. Ahl, D. Tytko, P.-P. Choi, R. Egoavil, M. Schowalter, T. Mehrtens, K. Mueller-Caspary, J. Verbeeck, D. Raabe, J. Hertkorn, K. Engl, A. Rosenauer, Homogeneity and composition of AlInGaN: a multiprobe nanostructure study, Ultramicroscopy 156 (2015) 29–36.
[32] R.F. Egerton, Electron-energy-loss spectroscopy (EELS) (1993).
[33] K. Riegler, G. Kothleitner, EELS detection limits revisited: ruby—a case study, Ultramicroscopy 110 (2010) 1004–1013.